nanomaterials

MDPI

Article

$[NiEn_3](MoO_4)_{0.5}(WO_4)_{0.5}$ Co-Crystals as Single-Source Precursors for Ternary Refractory Ni–Mo–W Alloys

Polina S. Serebrennikova [1,2], Vladislav Y. Komarov [1,2], Aleksandr S. Sukhikh [1,2], Svetlana P. Khranenko [1], Andrey V. Zadesenets [1], Sergey A. Gromilov [1,2,*] and Kirill V. Yusenko [3,*]

[1] Nikolaev Institute of Inorganic Chemistry, Lavrentiev Avenue 3, 630090 Novosibirsk, Russia; polina.buneeva2015@yandex.ru (P.S.S.); komarov_v_y@ngs.ru (V.Y.K.); a_sukhikh@niic.nsc.ru (A.S.S.); khranenko@niic.nsc.ru (S.P.K.); zadesenets@niic.nsc.ru (A.V.Z.)
[2] Department of Physics, Novosibirsk State University, Pirogova Str. 2, 630090 Novosibirsk, Russia
[3] BAM Federal Institute for Materials Research and Testing, Richard-Willstätter Str. 11, 12489 Berlin, Germany
* Correspondence: grom@niic.nsc.ru (S.A.G.); kirill.yusenko@bam.de (K.V.Y.)

Abstract: The co-crystallisation of $[NiEn_3](NO_3)_2$ (En = ethylenediamine) with Na_2MoO_4 and Na_2WO_4 from a water solution results in the formation of $[NiEn_3](MoO_4)_{0.5}(WO_4)_{0.5}$ co-crystals. According to the X-ray diffraction analysis of eight single crystals, the parameters of the hexagonal unit cell (space group *P*–31*c*, *Z* = 2) vary in the following intervals: a = 9.2332(3)–9.2566(6); c = 9.9512(12)–9.9753(7) Å with the Mo/W ratio changing from 0.513(3)/0.487(3) to 0.078(4)/0.895(9). The thermal decomposition of $[NiEn_3](MoO_4)_{0.5}(WO_4)_{0.5}$ individual crystals obtained by co-crystallisation was performed in He and H_2 atmospheres. The ex situ X-ray study of thermal decomposition products shows the formation of nanocrystalline refractory alloys and carbide composites containing ternary Ni–Mo–W phases. The formation of carbon–nitride phases at certain stages of heating up to 1000 °C were shown.

Keywords: complex salts; single-source precursors; molybdate anion; tungstate anion; X-ray diffraction; thermal decomposition; multicomponent nanostructured alloys

Citation: Serebrennikova, P.S.; Komarov, V.Y.; Sukhikh, A.S.; Khranenko, S.P.; Zadesenets, A.V.; Gromilov, S.A.; Yusenko, K.V. $[NiEn_3](MoO_4)_{0.5}(WO_4)_{0.5}$ Co-Crystals as Single-Source Precursors for Ternary Refractory Ni–Mo–W Alloys. *Nanomaterials* **2021**, *11*, 3272. https://doi.org/10.3390/nano11123272

Academic Editors: P. Davide Cozzoli and Zhanxi Fan

Received: 9 November 2021
Accepted: 29 November 2021
Published: 1 December 2021

1. Introduction

The low-temperature preparation of binary alloys from single-source precursors has been studied in a large number of works in the last decade [1–18]. Binary alloys can be prepared for a large variety of refractory metals including Pt, Pd, Ir, Rh, and Os. The stoichiometry of the resulting alloys obtained by thermal decomposition is fixed by the composition of their precursors. The main drawback of this approach is the discrete composition of a single-source precursor which does not allow one to vary the alloy's composition in a broad range. In the last decade, we developed a strategy to access not only binary phases but also ternary and multicomponent alloys with variable compositions using the co-crystallisation of isoformular isostructural coordination compounds [17]. As an example, $[Ir(NH_3)_5Cl][OsCl_6]$ was proposed as a precursor for *hcp*–$Ir_{0.5}Os_{0.5}$; $[Ru(NH_3)_5Cl][IrCl_6]$—for $Ir_{0.5}Ru_{0.5}$; $[Ru(NH_3)_5Cl]_2[OsCl_6]Cl_2$—for *hcp*–$Os_{0.33}Ru_{0.67}$. It has also been shown that isoformular compounds are isostructural and can be co-crystallized from water solutions. Such an important finding allowed us to first prepare binary *fcc*- and *hcp*-structured Ir–Ru alloys in the whole range of compositions according to the following generalised chemical equilibria:

$$x[Ir(NH_3)_5Cl]^{2+} + (1-x)[Ru(NH_3)_5Cl]^{2+} + [IrCl_6]^{2-} \rightarrow [Ir_xRu_{1-x}(NH_3)_5Cl][IrCl_6]$$
$$[Ir_xRu_{1-x}(NH_3)_5Cl][IrCl_6] \rightarrow Ir_{0.5+x/2}Ru_{0.5-x/2}.$$

Subsequently, such an approach was extended to the ternary Ir–Ru–Os and multicomponent systems [19,20]:

$$x[Ir(NH_3)_5Cl]^{2+} + (1-x)[RuNH_3)_5Cl]^{2+} + y[OsCl_6]^{2-} + (1-y)[IrCl_6]^{2-} \rightarrow [Ir_xRu_{1-x}(NH_3)_5Cl][Os_yIr_{(1-y)}Cl_6];$$

thermal decomposition in H_2 flow: $[Ir_xRu_{1-x}(NH_3)_5Cl][Os_yIr_{(1-y)}Cl_6] \rightarrow Ir_{0.5+x/2-y/2}Ru_{0.5-x/2}Os_{y/2}$.

A single-source precursors' approach seems to be extremely productive for the preparation of nano-porous refractory alloys. A possibility to vary composition using co-crystallisation makes the approach even more powerful to access alloys in a broad range of concentrations. The application of alloys with carbide-forming elements might be the next step for the design of multicomponent refractory ultrahard materials [21]. Nevertheless, systems with refractory metals such as Mo, W, and Ta have barely been investigated due to their high affinity to oxygen and the difficulties they present in being reduced from MO_4^{2-} anions that are stable in water solutions. In the current study, we report an investigation of $[NiEn_3](MoO_4)_{0.5}(WO_4)_{0.5}$ (En = ethylenediamine, $H_2NCH_2CH_2NH_2$) which can be obtained by the co-crystallization of two individual isoformular complex salts $[NiEn_3]WO_4$ and $[NiEn_3]MoO_4$. The crystal structures of both parent compounds were previously reported in [22,23]. Both salts are isostructural with a number of phases with the general formula $[M'En_3]M''O_4$ (M' = Co, Ni, Cu, Zn, Cd; M'' = Cr, Mo, W, S). These phases can be considered as promising single-source precursors to access binary alloys as well as composite carbide and oxide materials using their thermal decomposition in a reductive (hydrogen) and oxidative (oxygen and air) atmosphere. Thermal decomposition can be performed not only by using a solid/gas interface but also solid-state reaction. Thus, $[NiEn_3]MoO_4$ can be decomposed using LiH as a reduction agent in solid state (in a He flow as protective atmosphere) at 1000 °C. Decomposition results in a formation of $MoNi_4$, Mo_2C, and $Ni_2Mo_4C_x$ mixture. The thermal decomposition of $[NiEn_3]WO_4$ in H_2 flow as a reducing agent at 410 °C results in a formation of an *hcp*-structured $Ni(C_x)$ interstitial alloy mixed with *bcc*-$W_{1-x}Ni_x$ [24]. At 510 °C, an additional *fcc*-$Ni_{1-x}W_x$ binary alloy was obtained. Double-carbide Ni_2W_4C was detected above 660 °C as was Ni_6W_6C at 860 °C. These phases were proposed as an active catalyst for the synthesis of carbon nanotubes and carbon nanofibres [25,26] and as cathode materials for the synthesis of hydrogen by water electrolysis [27]. It is expected that the thermolysis of the co-crystallization product (CCP) of $[NiEn_3]MoO_4$ and $[NiEn_3]WO_4$ can lead to the formation of ternary alloys and carbides.

In the current study, a series of $[NiEn_3](MoO_4)_{1-x}(WO_4)_x$ as single-source precursors for ternary refractory alloys were synthetized from water solutions. The slow co-crystallisation of isoformular isostructural $[NiEn_3]MoO_4$ and $[NiEn_3]WO_4$ from water solution results in the formation of not a single-phase precipitate but a number of single crystals with large variations in their composition. The quality of the resulting single crystals may lead us to perform a single-crystal X-ray diffraction study to refine the chemical composition of each individual crystal. Individual crystals were used as single-source precursors for ternary Ni–Mo–W alloys after their decomposition above 1000 °C.

2. Materials and Methods

Synthesis of $[NiEn_3](MoO_4)_{0.5}(WO_4)_{0.5}$: Here, 1 mmol $Ni(NO_3)_2 \cdot 6H_2O$ was dissolved in 15 mL H_2O. Then, 1M NaOH water solution was added to form colloidal $Ni(OH)_2$ precipitate. Formed solid $Ni(OH)_2$ was centrifugated (3 min, 3000 rpm) and washed 3 times with a 1:1 water:ethanol mixture. Fresh $Ni(OH)_2$ precipitate was dissolved in ethylenediamine, formed a dark red precipitate after 15–20 min, and was mixed with $Na_2WO_4 \cdot H_2O$ (0.5 mmol, 0.165 g) and Na_2MoO_4 (0.5 mmol, 0.165 g) in 5 mL water. After intensive stirring, the reaction mixture was placed in a desiccator with solid NaOH as a drying agent. After 2 days at room temperature, violet crystals were collected. The yield was 85–90%.

An in-house X-ray powder diffraction study was performed at room temperature using a SHIMADZU powder XRD-7000 diffractometer (Shimadzu, Kyoto, Japan) (CuKα—radiation, $\lambda_{K\alpha 1}$ = 1.5406 Å, Ni-filter) in the range from 5° to 70° 2θ with a step of 0.03°.

The salts-precursors and $[NiEn_3](MoO_4)_{0.5}(WO_4)_{0.5}$ crystals were slightly ground in an agate mortar with heptane and LaB_6 (SRM660a, a = 4.1569 Å) as the internal standard. The samples were placed as a thin layer on the polished side of a standard quartz cuvette. The diffraction pattern was indexed using single crystal data obtained for parent $[NiEn_3]MoO_4$ (sp. gr. $P3\text{-}1c$, cell parameters: a = 9.2425(5) Å, c = 9.9601(5) Å). The positions of single reflexes were fitted as Lorentz functions using the Fityk software (Marcin Wojdyr, Institue of High Pressure Physics, Warsaw, Poland) [28]. A piecewise linear polyline dependence $\Delta 2\theta(2\theta)$ was constructed from the positions of K_{a1}-components of LaB_6 reflexes, and then used to apply corrections to the measured 2θ position of 11 reflexes corresponding to the studied salts. The unit cell parameters (UCPs) obtained by the least squares refinement were a = 9.2451(5), c = 9.9682(8) Å (FWHM~0.25) for $[NiEn_3](MoO_4)_{0.5}(WO_4)_{0.5}$, a = 9.2348(4); c = 9.9199(4) Å (FWHM~0.1) for $[NiEn_3]MoO_4$; and a = 9.2601(3), c = 9.9781(5) Å (FWHM~0.2° 2θ) for $[NiEn_3]WO_4$ (sp. gr. $P3\text{-}1c$). All FWHM values are given for reflexes (302), 2θ~38°.

High-resolution synchrotron X-ray powder diffraction (PXRD). Diffraction patterns for powdered $[NiEn_3](MoO_4)_{0.5}(WO_4)_{0.5}$ and salts-precursors were recorded at a high-resolution ID22 beamline at the ESRF (λ = 0.354395 Å) [29]. The station was equipped with a nine-channel detector with silicon crystal analysers (each channel is offset relative to the next one by 2° 2θ, data from each channel were independently recorded, and the information was then summed with an integration step of 0.002°). The beam size was 2 × 1 mm^2. During the shooting process, the detector was moved in continuous scanning mode around the sample axis. The sample in powder form was placed and sealed in 0.2 mm borosilicate glass mark tubes (Hilgenberg GmbH, Malsfeld, Germany). During the measurement, samples were axially rotated to provide an additional misdirection of the crystallites. The FWHM of single reflexes was 0.04° 2θ at 10–15° 2θ. A slight splitting of the diffraction lines at the high diffraction angles was recorded. The splitting indicates the heterogeneity (see inserted diagram in Figure 1) of the crystallite composition. Similar broadness was previously detected using in-house PXRD, but the synchrotron study gives a much higher number of individual reflexes to be fitted (up to 53) with a much higher instrumental resolution. For the refinement of cell parameters, diffraction profiles were fitted using the Gauss function (Figure 1). Average cell parameters were refined as a = 9.2409(2), c = 9.9576(3) Å (FWHM~0.012) for $[NiEn_3](MoO_4)_{0.5}(WO_4)_{0.5}$, a = 9.2440(5), c = 9.9607(6) Å (FWHM~0.015) for $[NiEn_3]MoO_4$ and a = 9.2707(2), c = 9.9863(4) Å (FWHM~0.012° 2θ) for $[NiEn_3]WO_4$. All FWHM values are given for (112) reflexes at 2θ~6°.

The single-crystal X-ray diffractions (SCXRD) of individual single crystals (~0.1–0.2 mm) were performed using a Bruker Duo and Bruker X8 (MoKα—radiation, $\lambda_{K\alpha 1}$ = 0.70932 Å, graphite monochromator, focusing collimator 0.60FC, four—axial goniometer, CCD detector, resolution 512 × 512, pixel size—120 microns). The temperature of each investigated single crystal was kept at 298(2) K during SC-XRD analysis using an Oxford Cryosystems Cobra (Bruker DUO, Bruker AXS GmbH, Karlsruhe, Germany) and Oxford Cryosystems Cryostream 800plus (Bruker X8, Bruker AXS GmbH, Karlsruhe, Germany) open-flow nitrogen coolers. The integration of experimental intensities accounting for absorption was performed using the APEX2 software package [30]; the structures were solved using the ShelxT [31] and refined using the ShelxL software package [32] as well as the Olex2 graphical interface [33]. For this study, 7 single crystals were selected. The cell parameters of the studied single crystals are given in Table 1. For all crystals, the occupancies of the metal sites in anions were refined.

Structural data for $[NiEn3](MoO_4)_{1-x}(WO_4)_x$ single crystals with different values of x (№1 with x = 0.487(3), №5 with x = 0.673(4), №6 with x = 0.824(4) and №7 with x = 0.924(5)) were deposited into the CCDC database under 2113885, 2113886, 2113887, and 2113888, respectively. All data are freely available online at https://www.ccdc.cam.ac.uk/ (accessed on 1 December 2021).

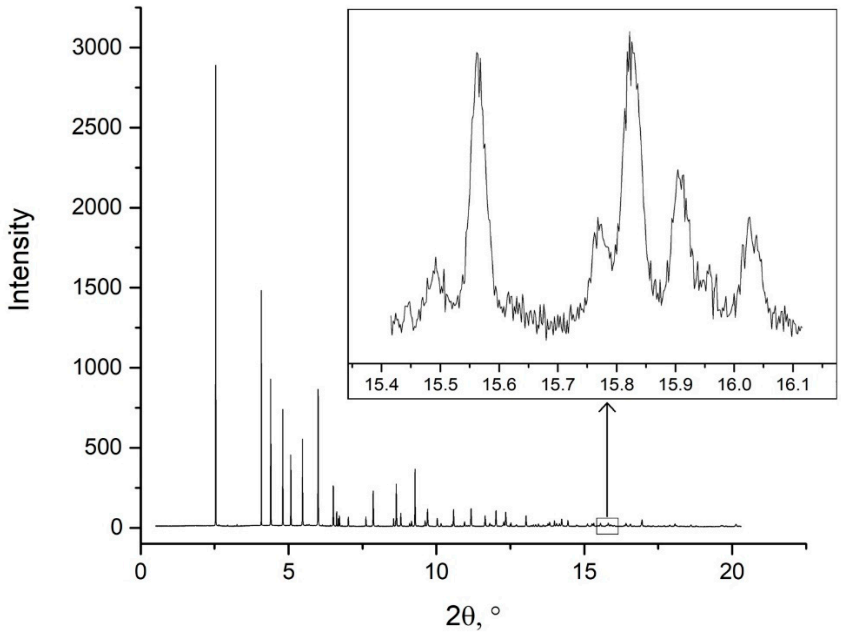

Figure 1. High-resolution synchrotron X-ray powder diffraction data (λ = 0.354395 Å) of $[NiEn_3](MoO_4)_{0.5}(WO_4)_{0.5}$. The inserted diagram shows the splitting of lines at the far angles' of diffraction.

Table 1. Results of the study of $[NiEn_3](MoO_4)_{1-x}(WO_4)_x$ individual single crystals *.

Number of the Crystal	1	2	3	4	5	6	7
CCDC database number	2113885	–	–	–	2113886	2113887	2113888
a, Å	9.2332(9)	9.2363(5)	9.2344(5)	9.2430(5)	9.2566(6)	9.2475(6)	9.2425(1)
c, Å	9.9512(12)	9.9582(5)	9.9577(6)	9.9590(5)	9.9753(7)	9.9639(8)	9.9682(2)
V, Å^3	734.7(2)	735.7(1)	735.6(1)	736.8(1)	740.2(1)	737.9(1)	737.4(2)
D_x, g/cm^3	1.996	2.007	2.014	2.030	2.056	2.122	2.163
θ interval, °	2.55–30.61	4.87–30.49	2.05–30.49	2.54–28.67	2.54–30.23	2.54–30.61	2.04–30.46
Completeness, %	100	95.8	98.67	97.35	100	100	100
$N_{parameters}$	43	43	43	43	43	43	43
S-factor by F^2	1.047	1.119	1.105	1.168	1.001	1.030	1.075
R_1 [$I > 2\sigma(I)$]	0.0133	0.0153	0.0168	0.0154	0.015	0.0114	0.0146
wR_2 [$I > 2\sigma(I)$]	0.0299	0.0308	0.0279	0.0347	0.0307	0.0264	0.0287
R_1 (all data)	0.0157	0.0174	0.0210	0.0175	0.0177	0.0133	0.0175
wR_2 (all data)	0.0310	0.0315	0.0286	0.0357	0.0314	0.0269	0.0295
x	0.487(3)	0.517(4)	0.536(4)	0.583(5)	0.673(4)	0.824(4)	0.924(5)

* $[NiEn_3]MoO_4$: *a* = 9.2425(5) Å, *c* = 9.9601(5) Å, *V* = 736.84(9) Å^3, *Z* = 2, sp. gr. *P*-31*c*; $[NiEn_3]WO_4$: *a* = 9.2641(3) Å, *c* = 9.9817(3) Å, *V* = 741.89(4) Å^3, *Z* = 2, sp. gr. *P*-31*c*.

The thermal decomposition of $[NiEn_3](MoO_4)_{0.5}(WO_4)_{0.5}$ was performed according to the protocol described in [24]. Briefly, several individual single crystals were mixed with LiH powder (1:1 volume ratio) and placed in a molybdenum crucible (outer diameter 3 mm; inner diameter 2 mm). A helium flow (99.995% purity) was used as protective atmosphere. Heating up to 1100 °C was carried out with 600°/min ramp, and the sample was kept at the final temperature for 1 min. The admixture of Li_2O was washed with distilled water.

A phase analysis was performed using a search-match in Powder Diffraction Files and International Crystal Structure Database [34,35].

The thermal decomposition of individual crystals was also performed in hydrogen flow. For the thermal decomposition, individual needle-shaped 1–2 mm single crystals were selected. Crystals №4 and №5 were heated in a hydrogen flow of up to 1000 °C with a heating rate of 10°/min and kept at the final temperature for 10 min. Crystals №2 and №3 were heated up to 1000 °C with a 10°/min ramp and tempered for 8 h at constant temperature. Mo/W ratios were obtained after the refinement of the single crystal X-ray diffraction data collected for 0.2 mm fragments of the same crystals.

The X-ray study of thermolysis products was carried out in the transmission geometry using a Bruker D8 Venture diffractometer (microfocus tube Incoteac IμS 3.0, Cu$K\alpha$ radiation, PHOTON 3 detector, resolution 768 × 1024, pixel size—135 microns; D = 69 mm; $2\theta_D$ = 45°). The detector position errors—distance D, angle 2θ and slopes were obtained from Si powder (SRM-640, a = 5.4309 Å) measurements and refined using the Dioptas software [36]. Cell parameters were refined from an additional measurement with D = 69 mm, $2\theta_D$ = 120°. The obtained phase composition and cell parameters are given in Table 2.

Table 2. The results of the X-ray phase analysis of thermal decomposition products (the crystal numbers correspond to the numbers from Table 1).

Conditions **Phase**	**T, °C** **t, min** **Gas**	**1000** **1** **He (LiH)**	**1000** **480** **H_2**	**1000** **480** **H_2**	**1000** **10** **H_2**	**1000** **10** **H_2**
N of sample.		№1	№2	№3	№4	№5
Ni/Mo/W mol. %		50/26/24	50/24/26	50/23/27	50/21/29	50/23/27
fcc (α) (*Fm*-3*m*)	a, Å	3.592(2)	–	–	3.587(2)	3.593(2)
	V_M, Å^3	11.586			11.538	11.596
bcc (β) (*Im*-3*m*)	a, Å	3.148(2)	3.154(2)	3.154(2)	3.153(2)	–
	V_M, Å^3	15.598	15.688	15.688	15.672	
(Mo,W)Ni$_4$ (γ) (*I*4/*m*)	a, Å	–	5.719(4)	5.719(4)	5.701(4)	–
	c, Å		3.588(2)	3.609(2)	3.574(2)	
	V_M, Å^3		11.735	11.804	11.616	
Ni$_2$(Mo,W)$_3$N$_x$ (a) ($P4_132$)	a, Å	–	–	–	6.633(4)	6.634(4)
	V_M, Å^3				14.592	14.598
Ni$_6$(Mo,W)$_6$C$_x$ (b) (*Fd*-3*m*)	a, Å	–	10.875(6)	10.884(6)	–	–
	V_M, Å^3		14.615	14.651		
Ni$_2$(Mo,W)$_4$C$_x$ (c) (*Fd*-3*m*)	a, Å	11.228(6)		–	–	–
	V_M, Å^3	16.085				

Ni: a = 3.5239 Å, V_M = 10.940 Å^3 [35; № 8688]; Mo: a = 3.1472 Å, V_M = 15.586 Å^3 [35; № 76147]; W: a = 3.1648 Å, V_M = 15.849 Å^3 [35; № 43421]; MoNi$_4$: a = 5.683, c = 3.592 Å, V_M = 11.61 [35; № 644017]; WNi$_4$: a = 5.730, c = 3.553 Å, V_M = 11.66 [34; № 03-065-2673]; Ni$_2$Mo$_3$N: a = 6.6340 Å, V_M = 14.598 Å^3 [35; № 50815]; Ni$_2$W$_3$N: a = 6.663 Å, V_M = 14.790 Å^3 [35; № 86170]; Ni$_6$Mo$_6$C: a = 10.891 Å, Z = 8, V_M = 13.456 Å^3 [35; 618328]; Ni$_6$W$_6$C: a = 10.873 Å, Z = 8, V_M = 14.607 Å^3 [35; 618588]; Ni$_2$Mo$_4$C: a = 11.250 Å, Z = 16, V_M = 14.832 Å^3 [35; 76137]; Ni$_6$W$_6$C: a = 11.226 Å, Z = 16, V_M = 14.607 Å^3 [35; 199847].

3. Results and Discussion

[NiEn$_3$]MoO$_4$ and [NiEn$_3$]WO$_4$ are isoformular and isostructural with close hexagonal cell parameters. Their crystal structures contain isolated octahedral cations $[NiEn_3]^{2+}$ and tetrahedral MO_4^{2-} anions (Figure 2). In the plane of the figure, each cation is surrounded by three anions with three identical M ... Ni distances of 5.34 Å. Additionally, in the coordination surroundings of the cation—the trigonal bipyramid—two additional anions are involved in the direction of the c axis at the distances of 4.979 Å. Anions have similar

surroundings. Thus, in the initial phase—the precursor—the metal atoms are mixed at the nanoscale.

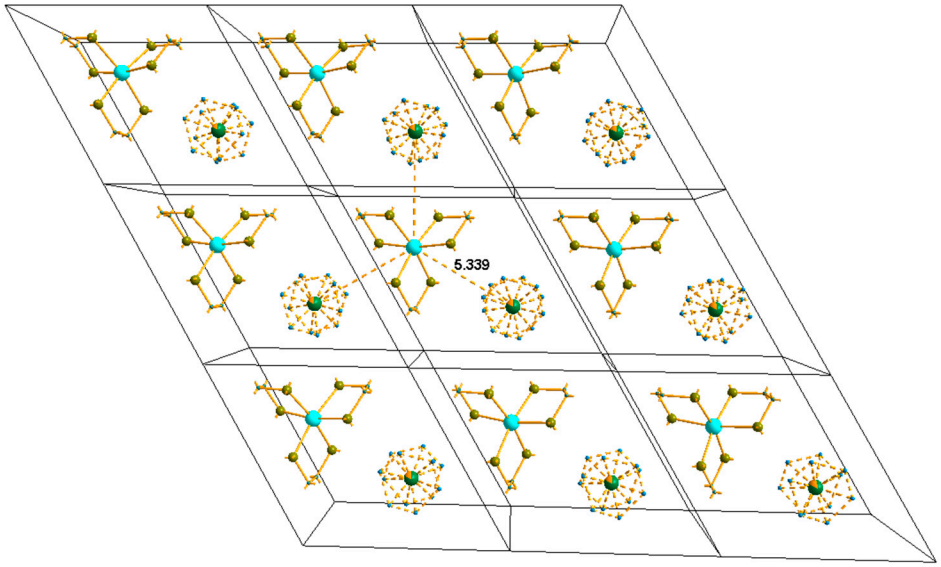

Figure 2. Model of anion disordering in a layer perpendicular to the *c* axis for crystal No 6. The Mo/W ratio is shown as a pie chart in the place of the corresponding atom (green is W and yellow is Mo).

All previous studies of multimetallic complex salts have been performed using powder X-ray diffraction. All multimetallic salts were prepared from isoformular isostructural salts with very similar cell parameters. In all studies, single-phase nature with the random metallic distribution of co-crystallised precursors similar to substitution in metallic solid solutions was postulated without an extensive analysis of the precursor's crystal structures and their possible inhomogeneity. Our preliminary PXRD study of bulk $[NiEn_3](MoO_4)_{0.5}(WO_4)_{0.5}$ material shows relatively broad diffraction lines. Such line-broadness might be explained by the low crystallinity of starting materials similar to those of previous works with multimetallic compounds and relatively low solubility [19,20,37]. In the current study, powder was prepared from ideal relatively large single crystals (up to several mm), where sample-specific line broadness seems to be negligible. It should also be noted that the FWHM of the lines in the diffraction pattern of the CCP turned out to be noticeably larger than the FWHM of the precursor salts. Theoretically, this broadening can be associated with the overlap of adjacent lines during the formation of a mechanical mixture of the initial phases which cannot be resolved due to the insufficient quality of laboratory diffraction data. This means that, according to the data of the laboratory powder diffraction study, it is impossible to conclude that the CCP is homogeneous. The powder diffraction study at the ID22 ESRF beamline allowed us to perform PXRD data collection using an instrument with one of the narrowest instrumental resolutions [26]. The average FWHM of the lines in the three obtained diffraction patterns coincide well and are smaller than in the case of the laboratory powder diffraction study. A visible splitting of the diffraction lines at the high-angle region was recorded. The splitting indicates the possible multiphase content of the powder. High-angle diffraction lines allow us to refine average cell parameters using the Gauss profile function as average a = 9.2409(2), c = 9.9576(3) Å (splitting was not taken into account while estimating the UCPs).

To prove our findings, several single crystals collected from the same synthesis were investigated. Each individual ideal single crystal seems to be homogeneous without a visible line broadness specific for low-crystalline materials. Nevertheless, there is significant variation in cell parameters between individual single crystals collected from the same bunch: a = 9.2332(3)−9.2566(6), c = 9.9512(12)−9.9753(7) Å; Mo/W ratio obtained from the

refinements of site occupancies changes from 0.513(3)/0.487(3) to 0.078(4)/0.895(9) (see details in Table 1).

The co-crystallisation from homogeneous equimolar solution occurs with large variations in unit cell parameters and crystal composition. Based on our findings, we can assume that the co-crystallisation of mixed salts with relatively low solubility such as $[Ru(NH_3)_5Cl][IrCl_6]$ and $[Ru(NH_3)_5Cl][IrCl_6]$, where solubility can be estimated as 10^{-3}–10^{-4} mol/L at room temperature in pure water, results in the fast crystallisation of homogeneous powder even from diluted solutions. In such a case, the concentration of the water solution directly controls the composition of the solid phase without the large enrichment of one component. The solubility of $[NiEn_3]MoO_4$ and $[NiEn_3]WO_4$ seems to be much higher and their crystallisation occurs from solutions with a relatively high concentration and viscosity. As a result, nucleation might occur with spontaneous enrichment with one component. A large number of seed crystals with variations in their composition form a large set of crystals with broad variations in their cell parameters and properties. Such a situation seems to be far from equilibrium, but further equilibration needs fast exchange between crystals through solution which probably need a long time with intensive stirring and/or heating. The described phenomena should play a critical role in the application of multimetallic salts as single-source precursors for multimetallic alloys. Indeed, if each crystal has its own composition and own crystal structure, inhomogeneous single-source precursors should form inhomogeneous alloys after decomposition.

Several individual single crystals were decomposed at 1000 °C in a H_2 flow (Table 2). The main phases in samples №4 and №5 were a double nitride based on the cubic Ni_2Mo_3N [35; № 50815] or isostructural Ni_2W_3N [35; № 86170]. The measured values of cubic cell parameter *a* and atomic volume (V_m) are closer to pure Ni_2Mo_3N. Nevertheless, one can also assume the formation of a non-stoichiometric phase with a lower nitrogen content. These ambiguities in the composition of double phases do not allow us to perform more precise quantitative phase analysis based on PXRD data. In addition, samples №4 and №5 revealed admixtures of *fcc*-structured alloys with cell parameters which were significantly larger in comparison with pure Ni, which is an indication of the formation of Ni alloyed with Mo and W (Figure 3).

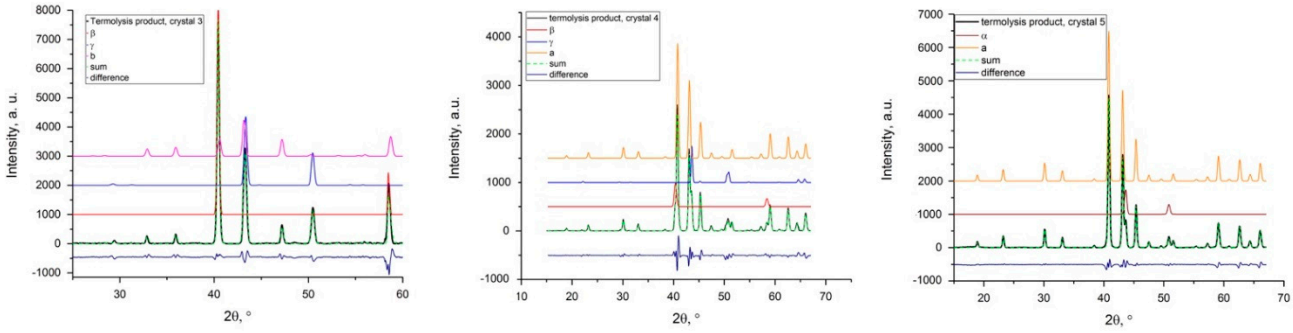

Figure 3. The results of the profile matching and cell parameters' refinement diffraction pattern corresponding to the thermolysis of crystals №3 (**left**), №4 (**middle**), and №5 (**right**) in H_2 (in-house single crystal diffractometer, MoKα−radiation, $\lambda_{K\alpha1}$ = 0.70932 Å). Metallic products contain *fcc*−structured alloy (α), *bcc*−structured alloy (β), $(Mo,W)Ni_4$ (γ), $Ni_2(Mo,W)_3N_x$ (a), and $Ni_6(Mo,W)_6C_x$ (b) phases. Inserts show original 2D diffraction images used for the integration of the patterns.

Additionally, sample №4 contains several minor admixtures such as a *bcc*-structured Mo- (or W-)-based alloy as well as $(Mo,W)Ni_4$ intermetallics. The *bcc*-phase has a cell parameter between Mo and W. According to the Ni–Mo and Ni–W binary phase diagrams, the maximal Ni solubility in the *bcc*-structured phase is 2 at. %. The Mo/W = 67/33 ratio in the *bcc*-phase can be estimated using Zen's law.

The atomic volume is defined as a ratio between the unit cell volume, V, and the number of atoms per unit cell, *Z* (*Z* = 2 for *bcc* and *Z* = 4 for *fcc*-structured alloys). According

to Zen's law [38], the atomic volumes, $V_M = V/Z$ (Å^3·atom^{-1}), for *bcc–fcc* bimetallic alloys, should follow a nearly linear dependence on composition with a relatively small positive or negative deviation [39]. For the (Mo,W)Ni_4 intermetallic phase, the Mo/W ratio was also estimated according to Zen's law based on atomic volumes (V_M) of $MoNi_4$ and WNi_4. The formation of partially disordered intermetallics and/or the inclusion of C and N atoms should be considered. The $MoNi_4$ phase was observed as a product of the thermal decomposition of [$NiEn_3$]MoO_4 with LiH at 1000 °C. The cell parameter a = 5.691 Å was significantly larger but the c = 3.577 Å and V_M = 11.58 Å^3·atom^{-1} were significantly smaller in comparison with the reference values refined as a = 5.683, c = 3.592 Å, and V_M = 11.66 Å^3·atom^{-1}.

The simultaneous decomposition of 10–15 [$NiEn_3$]$(MoO_4)_{0.5}(WO_4)_{0.5}$ crystals using LiH (~1:1 volume ratio) as a reducing agent at 1100 °C led to the formation of a three-phase mixture. The *Fcc*-structured phase based on the Ni lattice, *bcc*-structured phase based on Mo(W), as well as the ternary or four-component $Ni_2Mo_4(W)C_x$ carbide were observed (Table 2). In [24], a mixture of *fcc*-alloy (a = 3.583 Å) and $Ni_2W_4C_x$ (a = 11.200 Å) was observed after the thermal decomposition of [$NiEn_3$]WO_4 mixed with LiH under similar conditions. For [$NiEn_3$]MoO_4 mixed with LiH (He flow, 1050 °C, 1 min), a mixture of Mo_2C, $MoNi_4$ and $Ni_2Mo_4C_x$ phases was obtained.

After 8 h at 1000 °C, the phase composition of samples №2 and №3 significantly changed. The *bcc*-phase based on Mo (or W) and (Mo,W)Ni_4 were found to be the main phases. The intermetallic phase has abnormally large (relative to $MoNi_4$ and WNi_4) V_M values, which might be explained by the partial replacement of Ni by Mo and W, as well as the inclusion of C and N into the lattice. The $Ni_6(Mo,W)_6C$ phase was also detected as minor admixture in samples №2 and №3.

The unstable phase composition of samples obtained by holding the CCP at 1000 °C for 10 min can be explained by a small quantity of samples. This entails the irregularity in heat distribution inside the oven and as a result, the faster heating of sample №4 and the earlier appearance of β- and γ-phases. As shown in Table 2, the phase composition and the UCP satisfactorily coincide while increasing the exposure time to 480 min at 1000 °C. Subsequently, only these results are considered.

Figure 4 shows the cross-section of the ternary phase diagram for a temperature of 1000 °C, constructed of ternary diagrams of the Ni–Mo–W system [40–44] and binary diagrams [45,46], as well as taking into account the available experimental data [47,48]. The most recent Mo–Ni–W ternary phase diagram at 1000 °C is given in [44]. It was constructed by a combination of calculations using the CALPHAD and a limited array of experimental data (UCP and metal ratios) [43]. Figure 4 shows the regions of the existence of individual phases and their mixtures, as well as the regions of the compositions of precursors corresponding to our work and that of [44]. On the ternary phase diagram [40], the region corresponding to the specified compositions of precursors assumes the formation of a mixture of only α-and β-phases, while the (Mo,W)Ni_4 (γ-phase) is present on the binary Ni–Mo phase diagram only up to 870 °C. However, its presence in thermolysis products when they are heated up to 900 °C is shown in [44], and its appearance when heated up to 1000 °C is demonstrated in our work, so the corresponding area was plotted in Figure 4. Additionally, in the diagram for 1000 °C in [44], there is a region α + β + γ, which does not correspond to the data obtained in the current study. However, due to its rapid migration following an increase in the proportion of Mo with a decrease in temperature from 1000 to 900 °C and the presence of an error in setting the temperature in our experiment, this area cannot be taken into account while constructing the diagram.

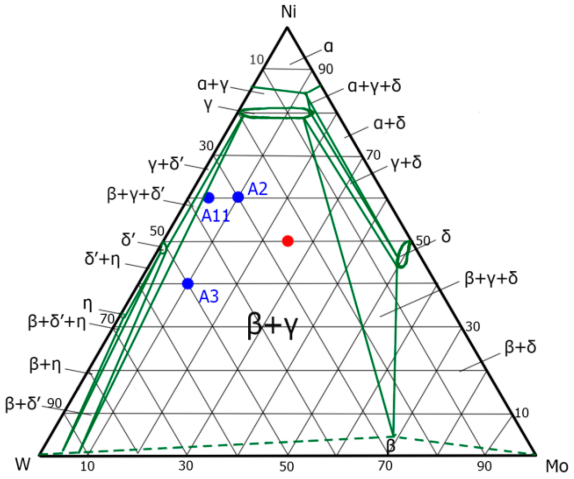

phase	symbol
fcc (*Fm*-3*m*)	α
bcc (*Im*-3*m*)	β
MoNi4 *I*4/*m*	γ
NiMo $P2_12_12_1$	δ
NiW $P2_12_12_1$	δ'
NiW2 *I*4	η

Figure 4. Ternary W–Mo–Ni (1000 °C isothermal cross-section). The red circle highlights the area of the initial atoms' ratio Ni/Mo/W studied in this work; the blue circles highlight the areas of the initial metal ratio of the samples from [44].

Table 3 shows a comparison of the data obtained by us with the data presented in [44]. While comparing the results of [44] with our data (Table 2), the presence of UCP differs in the second–third decimal place for *bcc*—and (Mo,W)Ni_4 phases can be seen. The values of point A11 are closest to our UCP, however, the initial ratios of the samples from [44] significantly differ from ours.

Table 3. The results of the X-ray phase analysis of thermal decomposition products.

Phase		A2 [43]	A3 [43]	A11 [43]	Current Work	
					№2	№3
Ni/Mo/W at. %		60/10/30	40/10/50	60/4/36	50/24/26	50/23/27
bcc (β) (I*m*-3*m*)	*a*, Å	3.14845	3.16408	3.16351	3.154(2)	3.154(2)
	V_M, Å^3	15.605	15.838	15.830	15.688	15.688
(Mo,W)Ni4 (γ) (*I*4/*m*)	*a*, Å	5.73774	5.70910	5.71754	5.719(4)	5.719(4)
	c, Å	3.55725	3.57707	3.57772	3.588(2)	3.609(2)
	V_M, Å^3	11.711	11.659	11.696	11.735	11.804

One should also take into account a possible formation of ternary Mo–Ni–C [49], W–Ni–C [50] carbides, and quaternary Mo–Ni–W–C [51].

4. Conclusions

Access to refractory alloys and ceramics based on W and Mo requires high temperature annealing or melting above 3000 °C. The works [52,53] show the formation of such alloys as a result of mechanochemical treatment for 20 h. Single-source precursors' strategy allows us to prepare not only ternary Mo–W–Ni alloys but also carbides and nitrides at relatively low temperatures below 1000 °C. Powder and single-crystal XRD study suggests that each homogeneous single crystal shows a large variety in composition, and as a result, various cell parameters. In this study, we show that it is important to more carefully study the products of co-crystallization, which in the future, are supposed to be applied as precursors in the production of metal phases.

The thermal decomposition of $[NiEn_3](MoO_4)_{0.5}(WO_4)_{0.5}$ in hydrogen flow at 1000 °C results in a formation of ternary Ni–Mo–W *fcc*- and *bcc*-structured alloys mixed with four component carbides and nitrides. Decomposition using solid LiH at 1000 °C results in

a formation of ternary alloys mixed with four-component cubic $Ni_2(Mo,W)_4C_x$ carbide, which does not form in H_2 flow, and no ordered phases were detected.

Author Contributions: Conceptualization and methodology, S.A.G.; investigation, data analysis and validation, P.S.S. and S.P.K.; X-ray diffraction data analysis, K.V.Y.; thermal decomposition, A.V.Z.; single-crystal data analysis, V.Y.K. and A.S.S.; original draft preparation, P.S.S., K.V.Y. and S.A.G. All authors contributed to writing and editing the manuscript. All authors have read and agreed to the published version of the manuscript.

Funding: This research received no external funding.

Acknowledgments: The authors thank the ID22 beamline at the European Synchrotron Radiation Facility, Grenoble, France, for providing us with the measurement time and technical support. The authors thank Ruslan Nikolaev (Nikolaev Institute of Inorganic Chemistry, Novosibirsk, Russia) for conducting the thermal decomposition with lithium hydride and Andy Fitch (ESRF, Grenoble, France) for assistance in conducting the experiment at the ID22 beamline. This research was supported by the Ministry of Science and Higher Education of the Russian Federation, N 121031700313-8.

Conflicts of Interest: The authors declare no conflict of interest.

References

1. Domonov, D.P.; Pechenyuk, S.I.; Belyaevskii, A.T.; Yusenko, K.V. Formation of nanostructured carbon from $[Ni(NH_3)_6]_3[Fe(CN)_6]_2$. *Nanomaterials* **2020**, *10*, 389. [CrossRef]
2. Kostin, G.A.; Filatov, E.Y.; Pischur, D.P.; Kuratieva, N.V.; Korenev, S.V. Phase transformations in a double complex salt of the ruthenium nitrosyl anion and tetraamine-palladium cation. *CrystEngComm* **2020**, *22*, 3692–3700. [CrossRef]
3. Filatov, E.; Lagunova, V.; Potemkin, D.; Kuratieva, N.; Zadesenets, A.; Plyusnin, P.; Gubanov, A.; Korenev, S. Tetraammineplatinum(II) and Tetraamminepalladium(II) Chromates as Precursors of Metal Oxide Catalysts. *Chem. Eur. J.* **2020**, *26*, 4341–4349. [CrossRef] [PubMed]
4. Berdyugin, S.; Volchek, V.; Asanova, T.; Kolesov, B.; Gerasimov, E.; Filatov, E.; Vasilchenko, D.; Korenev, S. Benzaldoxime to benzamide rearrangement catalysed by rhodium(III) hydroxocomplexes: The influence of polynuclear species. *Appl. Catal. A Gen.* **2019**, *587*, 117242. [CrossRef]
5. Korenev, S.V.; Venediktov, A.B.; Shubin, Y.V.; Gromilov, S.A.; Yusenko, K.V. Synthesis and structure of binarycomplexes of platinum group metals—Precursors of metallic materials. *J. Struct. Chem.* **2003**, *44*, 46–59. [CrossRef]
6. Vasilchenko, D.; Topchiyan, P.; Berdyugin, S.; Filatov, E.; Tkachev, S.; Baidina, I.; Komarov, V.; Slavinskaya, E.; Stadnichenko, A.; Gerasimov, E. Tetraalkylammonium Salts of Platinum Nitrato Complexes: Isolation, Structure, and Relevance to the Preparation of PtO_x/CeO_2 Catalysts for Low-Temperature CO Oxidation. *Inorg. Chem.* **2020**, *58*, 6075–6087. [CrossRef]
7. Yusenko, K.V.; Pechenyuk, S.I.; Vikulova, E.S.; Semushina, Y.P.; Baidina, I.A.; Filatov, E.Y. Isostructurality and Thermal Properties in the Series of Double Complex Salts $[M^1(NH_3)_6][M^2(C_2O_4)_3]\cdot 3H_2O$ (M^1 = Co, Ir, M^2 = Fe, Cr). *J. Struct. Chem.* **2019**, *60*, 1062–1071. [CrossRef]
8. Kostin, G.A.; Plyusnin, P.E.; Filatov, E.Y.; Kuratieva, N.V.; Vedyagin, A.A.; Kal'nyi, D.B. Double complex salts $[PdL_4][RuNO(NO_2)_4OH]$ (L = NH_3, Py) synthesis, structure and preparation of bimetallic metastable solid solution $Pd_{0.5}Ru_{0.5}$. *Polyhedron* **2019**, *159*, 217–225. [CrossRef]
9. Potemkin, D.I.; Filatov, E.Y.; Zadesenets, A.V.; Rogozhnikov, V.N.; Gerasimov, E.Y.; Snytnikov, P.V.; Korenev, S.V.; Sobyanin, V.A. Bimetallic Pt-Co/η-Al_2O_3/FeCrAl wire mesh composite catalyst prepared via double complex salt $[Pt(NH_3)_4][Co(C_2O_4)_2(H_2O)_2]\cdot 2H_2O$ decomposition. *Mater. Lett.* **2019**, *236*, 109–111. [CrossRef]
10. Filatov, E.Y.; Semushina, Y.P.; Gosteva, A.N. Obtaining and catalytic properties investigation of the products of double-complex salts $[Cr(ur)_6][M(L)_6]$ thermal oxidation (M = Co, Fe; L = CN^-, $1/2C_2O4^{2-}$). *J. Therm. Anal. Calorim.* **2018**, *134*, 355–361. [CrossRef]
11. Gosteva, A.N.; Plyusnin, P.E.; Semushina, Y.P.; Pechenyuk, S.I.; Filatov, E.Y.; Kyrtova, O.Y. The thermal behavior of double complex compounds with the cation $[Cr(ur)_6]^{3+}$ in a reducing atmosphere. *J. Therm. Anal. Calorim.* **2018**, *134*, 253–260. [CrossRef]
12. Zadesenets, A.V.; Filatov, E.Y.; Plyusnin, P.E.; Asanova, T.I.; Korolkov, I.V.; Baidina, I.A.; Shlyakhova, E.V.; Asanov, I.P.; Korenev, S.V. Complex salts of Pd(II) and Pt(II) with Co(II) and Ni(II) aqua-cations as single-source precursors for bimetallic nanoalloys and mixed oxides. *New J. Chem.* **2018**, *42*, 8843–8850. [CrossRef]
13. Domonov, D.P.; Pechenyuk, S.I.; Semushina, Y.P.; Kadyrova, G.I. Solid-state transformations by thermal decomposition of $[Co(en)_3][Fe(C_2O_4)_3]$ in an inert atmosphere. *Thermochim. Acta* **2020**, *687*, 178578. [CrossRef]
14. Vasilchenko, D.; Topchiyan, P.; Baidina, I.; Korolkov, I.; Filatov, E.; Zvereva, V.; Plyusnin, P.; Slavinskaya, E.; Gerasimov, E. Double complex salts containing $[Pt(NO_3)_6]^{2-}$ anion and Rh(III) complex cations: Synthesis, structure and utilisation for preparing (Rh–Pt)/CeO_2 catalysts. *J. Mol. Struct.* **2020**, *1211*, 128108. [CrossRef]
15. Domonov, D.P.; Pechenyuk, S.I.; Semushina, Y.P.; Yusenko, K.V. Solid-state transformations in inner coordination sphere of $[Co(NH_3)_6][Fe(C_2O_4)_3]\cdot 3H_2O$ as a route to access catalytically active Co-Fe materials. *Materials* **2019**, *12*, 221. [CrossRef] [PubMed]

16. Pechenyuk, S.I.; Zolotarev, A.A.; Gosteva, A.N.; Domonov, D.P.; Shimkin, A.A. Crystal structures and thermal behaviour of double complex compounds incorporating the $[Cr\{CO(NH_2)_2\}_6]^{3+}$ cation. *J. Mol. Struct.* **2017**, *1147*, 388–396. [CrossRef]
17. Yusenko, K.V.; Khandarkhaeva, S.; Bykov, M.; Fedotenko, T.; Hanfland, M.; Sukhikh, A.; Gromilov, S.A.; Dubrovinsky, L.S. Face-centered cubic refractory alloys prepared from single-source precursors. *Materials* **2020**, *13*, 1418. [CrossRef] [PubMed]
18. Duan, Y.; Yu, Z.-Y.; Yang, L.; Zheng, L.-R.; Zhang, C.-T.; Yang, X.-T.; Gao, F.-Y.; Zhang, X.-L.; Yu, X.; Liu, R.; et al. Bimetallic nickel-molybdenum/tungsten nanoalloys for high-efficiency hydrogen oxidation catalysis in alkaline electrolytes. *Nat. Commun.* **2020**, *11*, 1–10. [CrossRef]
19. Yusenko, K.V.; Riva, S.; Carvalho, P.A.; Yusenko, M.V.; Arnaboldi, S.; Sukhikh, A.; Hanfland, M.; Gromilov, S.A. First hexagonal close packed high-entropy alloy with outstanding stability under extreme conditions and electrocatalytic activity for methanol oxidation. *Scripta. Mater.* **2017**, *138*, 22–27. [CrossRef]
20. Yusenko, K.V.; Martynova, S.A.; Khandarkhaeva, S.; Fedotenko, T.; Glazyrin, K.; Koemets, E.; Bykov, M.; Smekhova, A.; Siemensmeyer, K.; Hanfland, M.; et al. High compressibility of synthetic analogous of binary iridium–ruthenium and ternary iridium–osmium–ruthenium minerals. *Materialia* **2020**, *14*, 100920. [CrossRef]
21. Ivanovskii, A.L. Platinum group metal nitrides and carbides: Synthesis, properties and simulation. *Russ. Chem. Rev.* **2009**, *78*, 303–318. [CrossRef]
22. Sukhikh, A.S.; Khranenko, S.P.; Komarov, V.Y.; Pishchur, D.P.; Nikolaev, R.E.; Buneeva, P.S.; Plyusnin, P.E.; Gromilov, S.A. $[Ni\mathit{En}_3]MoO_4$: Features of the phase transition and thermal decomposition in the presence of lithium hydride. *J. Struct. Chem.* **2019**, *60*, 780–788. [CrossRef]
23. Khranenko, S.P.; Sukhikh, A.S.; Pishchur, D.P.; Buneeva, P.S.; Komarov, V.Y.; Gromilov, S.A. $[Ni\mathit{En}_3]WO_4$. Crystal structural features of the phase transition at 269 K. *J. Struct. Chem.* **2018**, *59*, 1897–1902. [CrossRef]
24. Gromilov, S.A.; Gerasimov, E.Y.; Nikolaev, R.E. Formation of metallic and carbide phases via codecomposition of $[NiEn_3]WO_4$ and lithium hydride in the range 410–1060 °C. *Inorg. Mater.* **2019**, *55*, 331–336. [CrossRef]
25. Ago, H.; Uehara, N.; Yoshihara, N.; Tsuji, M.; Yumura, M.; Tomonaga, N.; Setoguchi, T. Gas analysis of the CVD process for high yield growth of carbon nanotubes over metal-supported catalysts. *Carbon* **2006**, *44*, 2912–2918. [CrossRef]
26. Bauman, Y.I.; Mishakov, I.V.; Rudneva, Y.V.; Plyusnin, P.E.; Shubin, Y.V.; Korneev, D.V.; Vedyagin, A.A. Formation of active sites of carbon nanofibers growth in self-organizing Ni–Pd catalyst during hydrogen-assisted decomposition of 1, 2-dichloroethane. *Ind. Eng. Chem. Res.* **2018**, *58*, 685–694. [CrossRef]
27. Kozin, L.F.; Volkov, S.V. *Modern Energy and Ecology: Problems and Prospects*; Naukova Dumka: Kiev, Ukraine, 2006. (In Russian)
28. Wojdyr, M. Fityk: A general-purpose peak fitting program. *J. Appl. Crystallogr.* **2010**, *43*, 1126–1128. [CrossRef]
29. ID22—High Resolution Powder Diffraction Beamline. Available online: https://www.esrf.eu/id22 (accessed on 6 August 2021).
30. Bruker AXS Inc. *APEX2 V2013.6-2, SAINT V8.32B and SADABS-2012/1*; Bruker Advanced X-Ray Solutions: Madison, WI, USA, 2012.
31. Sheldrick, G.M. Crystal structure solution with ShelXT. *Acta Crystallogr. Sect. A Found. Adv.* **2015**, *A71*, 3–8. [CrossRef] [PubMed]
32. Sheldrick, G.M. Crystal structure refinement with SHELXL. *Acta Crystallogr. Sect. C Struct. Chem.* **2015**, *71*, 3–8. [CrossRef] [PubMed]
33. Dolomanov, O.V.; Bourhis, L.J.; Gildea, R.J.; Howard, J.A.; Puschmann, H. OLEX2: A complete structure solution, refinement and analysis program. *J. Appl. Crystallogr* **2009**, *42*, 339–341. [CrossRef]
34. *Powder Diffraction File: PDF-2*; International Centre for Diffraction Data: Newtown Square, PA, USA, 2021.
35. *Inorganic Crystal Structure Database. D–1754*; FIZ Karlsruhe—Leibniz Institute for Information Infrastructure: Eggenstein–Leopoldshafen, Germany, 2021.
36. Prescher, C.; Prakapenka, V.B. DIOPTAS: A program for reduction of two-dimensional X-ray diffraction data and data exploration. *High Press. Res.* **2015**, *35*, 223–230. [CrossRef]
37. Yusenko, K.V.; Bykova, E.; Riva, S.; Bykov, M.; Crichton, W.A.; Yusenko, M.V.; Sukhikh, A.; Arnaboldi, S.; Hanfland, M.; Dubrovinsky, L.S.; et al. Ir–Re binary alloys under extreme conditions and their electrocatalytic activity in methanol oxidation. *Acta Mater.* **2017**, *139*, 236–243. [CrossRef]
38. Zen, E.-a. Validity of "Vegard's Law". *Am. Mineral.* **1956**, *41*, 523–524.
39. Denton, A.R.; Ashcroft, N.W. Vegard's law. *Phys. Rev. A* **1991**, *43*, 3161–3164. [CrossRef] [PubMed]
40. Gupta, K.P. The Mo-Ni-W (Molybdenum-Nickel-Tungsten) System. *Phase Diagr. Ternary Nickel Alloy.* **1991**, *2*, 134–147.
41. Udovskii, A.L. Computer Modelling of Phase Diagrams, Thermodynamic Properties, and Structure of Multicomponent Systems. *Russ. Metall.* **1990**, *2*, 132–153.
42. Zhang, C.; Liu, Y.; Du, Y.; Peng, Y.; Wang, J. Thermodynamic Assessment of the Co-Mo-Ni and Mo-Ni-W Ternary Systems. *CALPHAD Comput. Coupling Phase Diagr. Thermochem.* **2016**, *55*, 243–251. [CrossRef]
43. Maslenkov, S.B.; Nikandrova, E.A. Examination of the Ni–Mo–W Phase Diagram. *Russ. Metall.* **1980**, *2*, 184–187.
44. Tang, M.; Du, Y.; Zhou, P.; Wang, S.; Zhang, H.; Zeng, Y.; Liu, S.; Chai, X.; Peng, Y.; Wu, C.; et al. Experimental phase diagram, thermodynamic modeling and solidified microstructure in the Mo–Ni–W ternary system. *CALPHAD Comput. Coupling Phase Diagr. Thermochem.* **2020**, *68*, 101748. [CrossRef]
45. Frisk, K. A thermodynamic evaluation of the Mo–Ni system. *CALPHAD Comput. Coupling Phase Diagr. Thermochem.* **1990**, *14*, 311–320. [CrossRef]

46. Gustafson, P. An experimental study and a thermodynamic evaluation of the Fe–Mo–W system. *Int. J. Mater. Res.* **1988**, *79*, 388–396. [CrossRef]
47. Novichkova, O.V.; Kaputkin, I.I.; Uljyanin, E.A. Features of the Phase Composition of Nickel Alloys with High Tungsten and Molybdenum Contents. *Met. Sci. Heat Treat.* **1989**, *31*, 895–899. [CrossRef]
48. Arapova, L.P.; Mostovetskaya, A.P. Ordering Kinetics in Alloys of Nickel with Tungsten and Molybdenum at T = 800 °C. *Izv. Vyss. Uchebn. Zaved. Fiz.* **1990**, *33*, 78–82. (In Russian) [CrossRef]
49. Zhang, C.; Peng, Y.; Zhou, P.; Du, Y. Thermodynamic modeling of the C-Co-Mo and C-Mo-Ni ternary systems. *J. Phase Equilibria Diffus.* **2016**, *37*, 423–437. [CrossRef]
50. Fernandes, C.M.; Senos, A.M.R. Cemented carbide phase diagrams: A review. *Int. J. Refract. Met. Hard Mater.* **2011**, *29*, 405–418. [CrossRef]
51. Inoue, A.; Naohara, T.; Masumoto, T.; Kumada, K. Thermal stability and hardness of new type nickel-based alloys amorphous alloys. *Trans. Jpn. Inst. Met.* **1979**, *20*, 577–584. [CrossRef]
52. Liu, X.J.; Hu, H.H.; Hana, J.J.; Lua, Y.; Wang, C.P. Assessment of the diffusional mobilities in *fcc* Ni–Nb and *fcc* Ni–Mo alloys. *CALPHAD Comput. Coupling Phase Diagr. Thermochem.* **2020**, *38*, 140–145. [CrossRef]
53. Patra, A.; Karak, S.K.; Pal, S. Synthesis and Characterization of $W_{80}Ni_{10}Mo_{10}$ alloy produced by mechanical alloying. *IOP Conf. Ser. Mater. Sci. Eng.* **2015**, *75*, 012032. [CrossRef]